euspen's 24th International Conference & Exhibition, Dublin, IE, June 2024
www.euspen.eu

Mechanical resonance induced measurement uncertainty of ultra-precision on-machine surface measurement system

Maomao Wang, Wenbin Zhong*, Guoyu Yu, Paul Scott, Xiangqian Jiang, Wenhan Zeng

EPSRC Future Metrology Hub, Centre for Precision Technologies, University of Huddersfield, Huddersfield, HD1 3DH, UK

**Corresponding author: W.Zhong@hud.ac.uk*

Abstract

Mechanical vibration is an inevitable factor for on-machine surface measurement (OMSM), and it can significantly impact the measurement results, particularly when measuring high-sag surfaces. A great number of OMSM system has been reported in recent decades, however, the contribution of the mechanical resonance on the measurement result has never been revealed. This paper investigates the source of measurement uncertainty arising from mechanical resonance errors in the OMSM system. The system dynamic model of the whole measurement platform is modelled by an equivalent two degree of freedom (2-DOF) oscillating system. The frequency response property of on-machine measurement device fixture is evaluated experimentally by hammer excitation test. A case study on evaluation of large off axis spherical (OAS) with 380 mm diameter aperture is performed. Resonance condition is identified by a joint time-frequency analysis on the slide acceleration and the chromatic sensor displacement. A net-zero-force criteria is applied to locate the moments resonance happens. The on-machine measurement result indicates that time-variant force fluctuation of the precise slide is the major excitation source for the integrated measurement device. It shows that the disturbance induced by system resonance can reach up to 300 nm, which is 100 times greater than the ground truth amplitude in a quasi-static measurement. This research provides a potential solution for evaluating the real-world performance of optical measurement devices integrated with manufacturing equipment.

Keywords: In-process measurement, ultra-precision, uncertainty, vibration

1. Introduction

Integrating surface metrology devices with machining equipment is becoming highly focused in recent decades, as it helps to improve the metrology efficiency and machining quality of components [1]. Integrating a point measurement sensor on the axes of the lathe forming a coordinate measurement machine (CMM) is one of the most feasible solutions for ultra precision surface measurement [2]. It is crucial to perform careful alignment and calibration to get a reliable measurement result.

Attentions have been paid to mitigate the static errors, including axis kinematic errors [3], beam deviation induced errors [4], and temperature fluctuation induced errors [5]. Alignment between the point measurement sensor and the target surface is usually guaranteed by fine adjustment mechanisms [6]. Existing works regard mechanical vibration as a random noise introduced to the system [5]. However, the dynamic interaction between the platform and the integrated measurement device has seldomly been revealed.

In this paper, a system dynamics model is developed for the on-machine measurement system. The contribution of the mechanical resonance to the uncertainty of on machine measurement is studied. A case study of on machine evaluating a large sag off-axis sphere mirror is illustrated.

2. Measurement system and dynamics model

2.1. On machine measurement system

An OMSM system is setup on a diamond turning machine, as shown in Fig 1. The chromatic confocal sensor has nanometre level vertical resolution over 100 µm measurement range. The platform is a Moore Nanotech 650 FG-V2 diamond turning machine. The measurement system and machine control system are synchronized by an in-house developed controller HUD-CNC [7, 8].

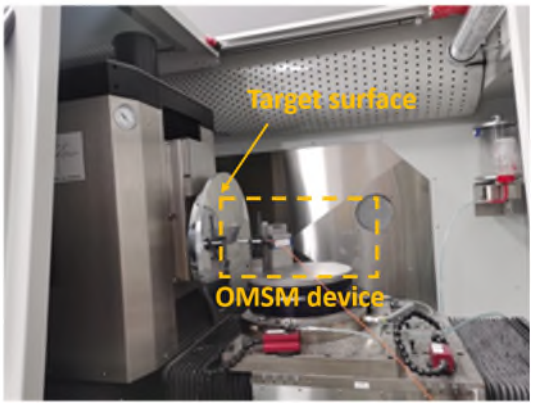

Figure 1. On machine measurement system.

The slide is driven by linear motors with hydrostatic bearings, and the sensor is mechanically coupled to the B-axis by an adjustable fixture. The accurate positions of the slides are measured by linear grating encoders for closed-loop control and large range coordinate measurement.

2.2. Dynamic property identification of OMSM device

The dynamic response of the OMSM unit is evaluated with the hammer impact experiment. The setup of the test system is shown in Fig 2. An impact hammer and an accelerometer are applied for the measurement of the impact input and response. The fixture is attached to a rigid steel bench and the sensitive direction of the accelerometer is in the horizontal plane. The impact signal and the acceleration signal are collected simultaneously by a NI-USB-6211 data acquisition card.

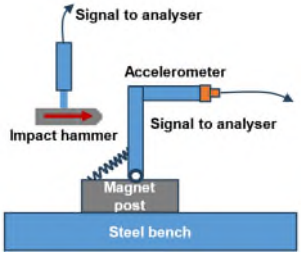

Figure 2. Schematic of nature frequency test of OMSM fixture.

The measured impact signal and response are shown in Fig 3. It can be identified that the first three order nature frequency of the OMSM device is 293Hz, 385Hz, 106Hz.

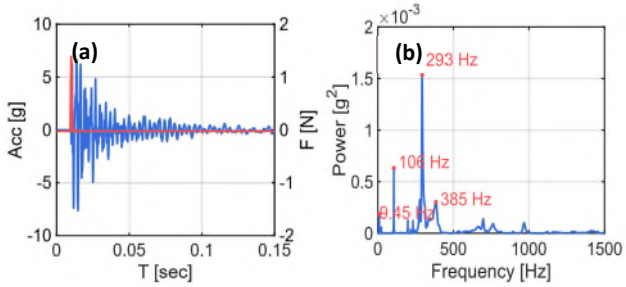

Figure 3. (a) Impact and response of the OMSM fixture, (b) Frequency spectrum of the response signal.

2.3. Dynamic model of the full OMSM system

Resonance of the OMSM system and the platform is a sensitive factor that affects the measurement result as the fixture is not ideally rigid. Dynamics model of the whole system is shown in Fig 4. The sensor is coupled to the stage by a fixture, and the stage is driven by a linear motor, and the corresponding driving force is F_d.

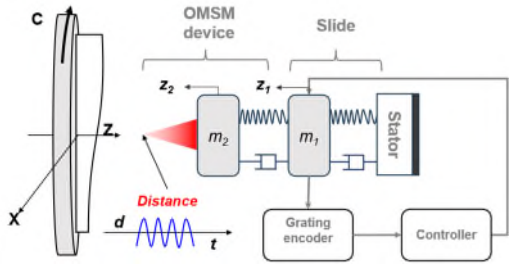

Figure 4. System dynamic model of the OMSM system integrated with diamond turning machine.

The dynamic system is simplified as 2-DOF oscillating system as shown in Fig 4. The state space model of the system is:

$$\dot{x} = \boldsymbol{A}x + \boldsymbol{B}u \tag{1}$$

$$\dot{y} = \boldsymbol{C}x + \boldsymbol{D}u \tag{2}$$

where $\boldsymbol{A}$, $\boldsymbol{B}$, $\boldsymbol{C}$ and $\boldsymbol{D}$ are the coefficients determined by the mechanical components of the system, and $\dot{x}$, $\dot{y}$ and u are state variable. The measurement device integrated with the stage is a mechanical system with time-invariant parameters, thus $\boldsymbol{D}$ is zero in this study. The model can be expressed in a form with parameters:

$$\begin{bmatrix} \dot{x}_1 \\ \ddot{x}_1 \\ \dot{x}_2 \\ \ddot{x}_2 \end{bmatrix} = \begin{bmatrix} 0 & 1 & 0 & 0 \\ \frac{k_1}{m_1} & \frac{b_1}{m_1} & -\frac{k_1+k_2}{m_1} & -\frac{b_1+b_2}{m_1} \\ 0 & 0 & 0 & 1 \\ -\frac{k_1}{m_2} & -\frac{b_1}{m2} & \frac{k_2}{m_2} & \frac{b_2}{m_2} \end{bmatrix} \begin{bmatrix} x_1 \\ \dot{x}_1 \\ x_2 \\ \dot{x}_2 \end{bmatrix} + \begin{bmatrix} 1/m_1 \\ 0 \\ 0 \\ 0 \end{bmatrix} F_d \tag{3}$$

$$y = \begin{bmatrix} 1 & 0 & 0 & 0 \\ 0 & 0 & 1 & 0 \end{bmatrix} \begin{bmatrix} x_1 \\ \dot{x}_1 \\ x_2 \\ \dot{x}_2 \end{bmatrix} \tag{4}$$

where x_1 and x_2 are the absolute position of the slide and the OMSM sensor, respectively. F_d is the driving force from the linear motor. Physical meaning and values of other parameters are listed in the table below. The stiffness of the slide and the mass of the OMSM fixture are explicitly given in the table. Other parameters need to be practically determined. More detailed analysis on the similar system can refer to [9, 10].

Table 1. Parameters of system dynamics.

Parameters		Units	Variable name	Value
Slide	Mass	kg	m_1	*
	Stiffness	N/μm	k_1	200
	Damp	1	c_1	*
OMSM fixture	Mass	Kg	m_2	0.5
	Stiffness	N/μm	k_2	*
	Damp	1	c_2	*
*Parameters practically determined				

The state of the system can be solved numerically with the explicit Runge-Kutta method with all parameters are determined. Here, two major semiquantitative conclusions can be assumed for further analysis of the system:

a) For forced vibration, the system response frequency f is governed by the frequency of the driving force f_d.

b) When mechanical resonance occurs, the force on the slide fulfils the relationship:

$$F_{Net} = F_{21} + F_d = 0 \tag{5}$$

where F_{21} is the interaction force between the slide and the OMSM fixture. As the position of the slide z_1 is measured by a precision grating encoder with very high resolution, thus with the help of Eq (5), we can simplify the analysis by estimating the net force:

$$F_{Net}/m_1 = \ddot{z_1} \tag{6}$$

2.4. Frequency response and uncertainty of the system

The OMSM system is configured with a CMM structure, thus for an ideal measurement:

$$z_1(t) = z_2(t),\ z(t) = d(t) + z_1(t) \tag{7}$$

where $d(t)$ is the true position of the target, considering the error contributed to the vibration of the system:

$$z_2(t) = z_1(t) + \delta(t),\ \overline{z(t)} = d(t) + z_1(t) + \delta(t) \tag{8}$$

where $\boldsymbol{\delta}(t)$ is the relative displacement between the sensor and the slide of the machine. The dynamic effect induced measurement error is defined as:

$$Ez = \overline{z(t)} - z(t) = \delta(t) \tag{9}$$

There is only one active force in the system, the driving force of the motor upon the slide. It can be summarized that variation of the driving force on the slide is the governing factor that affects the measurement error, which causes a forced vibration of the OMSM system. And according to the properties of the forced vibration, two major contributions of the error caused by vibration:

a) Frequency of driving force is close to the nature frequency of OMSM system fixture.
b) Wide bandwidth stochastic background noise exists in the driving force.

3. Case study: On machine measurement of large sag OAS

A large area off axis spherical surface (OAS) is fabricated with the diamond turning machine as shown by Fig 5. The curvature radius is 5000 mm, the aperture diameter is 380 mm, and the sag value is 5 mm. Due to the sag value is much greater than the range of the chromatic confocal sensor, the *Z* axis of the machine is incorporated to enlarge the measurement range.

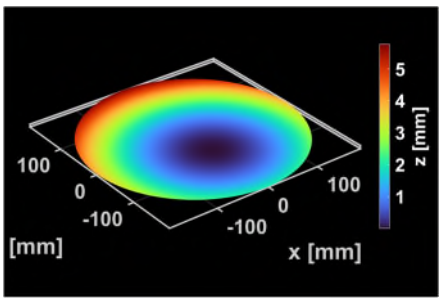

Figure 5. Topography off-axis sphere measured by OMSM method.

3.1 Quasi-static distance measurement

A quasi-static measurement of 30 seconds is performed to identify the background noise of the measurement system when all axis are standstill. The time series measurement result and the power spectral density (PSD) are shown in Fig 6(a) and (b). The absolute amplitude of the noise is about 50 nm. The major components of the measurement results are high frequency noise of 320 Hz with a root means square (RMS) of 3.16 nm. Some minor frequency components are also identified near the 200 Hz and 100 Hz and 50 Hz, respectively. The results indicate that the chromatic confocal sensor integrated with the system is qualified for evaluating surface form, sufficient in most cases to measure waviness, and may not be accurate in roughness evaluation.

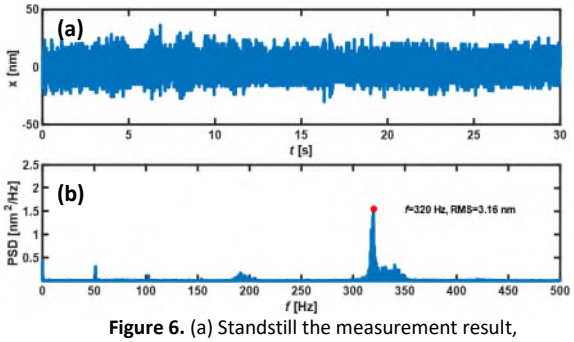

Figure 6. (a) Standstill the measurement result,
(b) PSD of the standstill measurement signal.

3.2 Uncertainty evaluation method

The deviation between the ground truth value and the measured results is given in Eq (9). Due to the ground truth of the on-machine measurement is unknown, the contribution of the vibration is evaluated by:

$$\hat{\delta}(t) = z(t) - z'(t) \tag{10}$$

where $z(t)$ is the original measured profile, $z'(t)$ is the profile filtered by a robust median filter with 32 points fixed bandwidth. Fig 7 (a) shows part of the continuous evaluation profile. The deviation between $z(t)$ and $z'(t)$changes over the time. It can be identified that the maximum deviation happens at the moment of 1.35 hours.

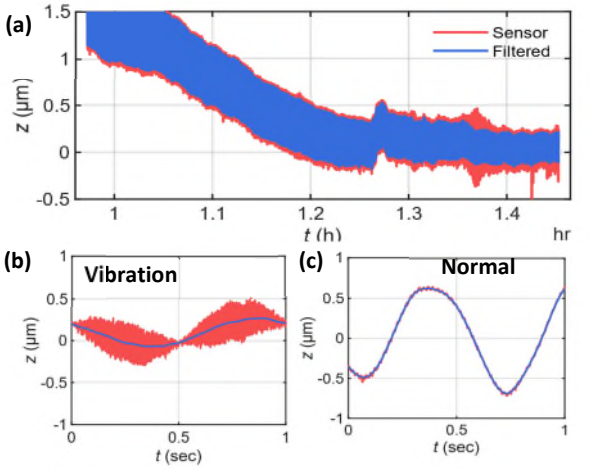

Figure 7. (a) On machine measured profile,
(b) Measured profile with vibration,
(c) Measured profile under normal conditions.

One single circular profile at that moment is extracted in 1 second, the peak-to-valley(P-V) value of the original profile is about 0.8 μm. The P-V value of the filtered high frequency signal is about 0.5 μm, nearly the same level of the surface form, which is far beyond reliable. In comparison with the profile measured at normal condition, the P-V value of the high frequency components is within tens of nanometers, the same level of system background noise. The relative error contributed by the vibration is indicated by:

$$Err = \frac{\mathbf{PV}[z(t)] - \mathbf{PV}[z'(t)]}{\mathbf{PV}[z(t)]} \tag{11}$$

For a frequency component, the absolute contribution of the vibration to the profile is given by:

$$\mathrm{RMS}(f) = \int_{f_1}^{f_2} \frac{\mathrm{FFT}\left(\hat{\delta}(t)\right)^2}{Bw} \mathrm{d}f \tag{12}$$

where $\mathrm{FFT}(\cdot)$ is the fast Fourier transform spectrum of the separated profile, and Bw is the bandwidth of the filtered profile, which is the range between cutoff frequency f_L to $F_s/2$.

3.3 Full time scope evaluation on vibration

The full scanned profile Z_2 is evaluated with time-frequency analysis method, and the time spectrum is shown in Fig 8. The form is removed with a low pass filter. In total five different time windows, and for each the duration is shown in detail. A background stationary vibration about 50 Hz, 200Hz, and 330 Hz is shown in the chart. The 50 Hz is close to the working current of the motor, and the other two frequencies are located within the range of the nature frequency of the OMSM fixture.

Resonance vibration occurred from 1.1 hour to 1.5 hour. A series of time variant frequency components are identified. Three resonance moments are identified at T_2, T_4, and T_5. The frequencies are 420 Hz, 350Hz, and 180 Hz, respectively. The distortion on the P-V values is 0.02 μm, 0.1 μm, 0.5 μm, respectively. The absolute contribution of the resonance vibration to the overall amplitude of the measurement are: RMS(f_{420Hz})=50 nm, RMS(f_{350Hz})=200 nm, RMS(f_{180Hz})=300 nm. A series of higher order vibration components over 400 Hz is identified after 1.3 hours, limited by the measurement bandwidth of the sensor, these components current is hard to

be interpreted. One major concern of the mode identification problem illustrated here is how to avoid accounting surface waviness in the evaluation results. Here, the analysing technique is referred to as zero-net-force criterium is applied, and the details are shown in the following section.

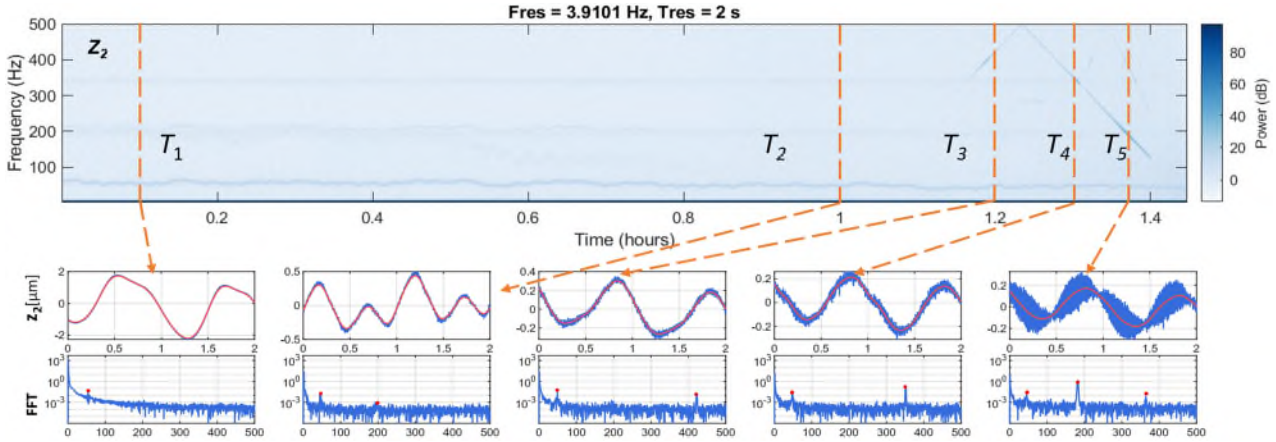

Figure 8. Time-frequency analysis of the full time scope profile measured by OMSM.

3.4 Zero net force criteria for resonance identification

As the conclusion implied by Eq (5) in Sec 2.3, the zero net force criteria are applicable to identifying the moment resonance happens in a forced vibration. Fig 9 shows the time-frequency properties of the net force on the slide, as well as the response of the OMSM sensor. It can be identified from the frequency of response follows the disturbance on the net force. Two notches on the time-frequency diagram of the net force are identified.

Among them, Notch1-Vr1, Notch2-Vr2 are two pairs of resonance modes in the system, which is shown in Fig 9(a) and (b). Vr1 and Vr2 located the frequency of OMSM fixture nature frequency range. Vr3=320 Hz is same as the main frequency components of the background noise of the system.

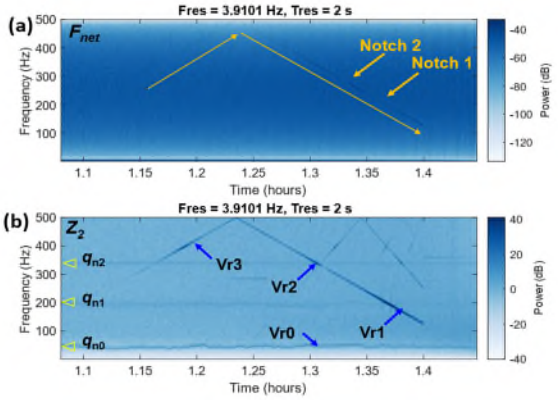

Figure 9. (a) Time-frequency diagram of net force on the slide, (b) Time-frequency diagram of the position of OMSM sensor, q_{n0} is the background noise, and q_{n1}, q_{n2} are the first two order nature frequencies of the OMSM fixture.

4. Summary and conclusions

In this paper, we firstly present the measurement uncertainty caused by mechanical resonance for on machine measurement system. Due to the disturbance of the platform, the result from the point measurement sensor is distorted with an amplitude of 0.5 μm over a millimetre scale surface measurement. The system dynamics model is established to evaluate the contribution of the resonance vibration to the measurement result. The results indicate that the disturbance induced by system resonance can be 100 times greater than the ground truth amplitude in a quasi-static measurement. This research will contribute to a more comprehensive understanding of the performance of optical measurement devices integrated with manufacturing equipment.

Declaration of Competing Interest

The authors declare that they have no known competing financial interests or personal relationships that could have appeared to influence the work reported in this paper.

Acknowledgment

The authors gratefully acknowledge the UK's EPSRC funding of Future Metrology Hub (Ref: EP/P006930/1), and the UK's STFC-IPS funding (Grant Ref: ST/W005263/1).

References

[1] Li, D., Wang, B., Tong, Z., Blunt, L., and Jiang, X.: 'On-machine surface measurement and applications for ultra-precision machining: a state-of-the-art review', The International Journal of Advanced Manufacturing Technology, 2019, 104, (1-4), pp. 831-847

[2] Rolland, J.P., Davies, M.A., Suleski, T.J., Evans, C., Bauer, A., Lambropoulos, J.C., and Falaggis, K.: 'Freeform optics for imaging', Optica, 2021, 8, (2), pp. 161-176

[3] Li, D., Tong, Z., Jiang, X., Blunt, L., and Gao, F.: 'Calibration of an interferometric on-machine probing system on an ultra-precision turning machine', Measurement, 2018, 118, pp. 96-104

[4] Xi, M., Wang, Y., Liu, H., Xiao, H., Li, X., Li, H., Ding, Z., and Jia, Z.: 'Calibration of beam vector deviation for four-axis precision on-machine measurement using chromatic confocal probe', Measurement, 2022, 194, pp. 111011

[5] Ye, L., Qian, J., Haitjema, H., and Reynaerts, D.: 'Uncertainty evaluation of an on-machine chromatic confocal measurement system', Measurement, 2023, 216, pp. 112995

[6] Wang, S., and Zhao, Q.: 'Development of an on-machine measurement system with chromatic confocal probe for measuring the profile error of off-axis biconical free-form optics in ultra-precision grinding', Measurement, 2022, 202, pp. 111825

[7] Tong, Z., Zhong, W., Zeng, W., and Jiang, X.: 'Closed-loop form error measurement and compensation for FTS freeform machining', CIRP Annals, 2021, 70, (1), pp. 455-458

[8] Zhong, W., Tong, Z., and Jiang, X.: 'Integration of On-machine Surface Measurement into Fast Tool Servo Machining', Procedia CIRP, 2021, 101, pp. 238-241

[9] Altintas, Y., Verl, A., Brecher, C., Uriarte, L., and Pritschow, G.: 'Machine tool feed drives', Cirp Ann-Manuf Techn, 2011, 60, (2), pp. 779-796

[10] Huang, P., Wu, X., To, S., Zhu, L., and Zhu, Z.: 'Deterioration of form accuracy induced by servo dynamics errors and real-time compensation for slow tool servo diamond turning of complex-shaped optics', International Journal of Machine Tools and Manufacture, 2020, 154